Chapter 2
Optical Waveguides

Abstract This section describes the characteristics of optical waveguides in various material systems. The main focus will be on the properties of glass fiber whose different types and production methods will be described. The material systems of optical waveguides, which are described in this chapter, are displayed in the following: (1) in fibers, (2) in SiO_2, (3) in Polymethylmethacrylate (PMMA), (4) in GaAs, and (5) in InP.

2.1 The Most Important Optical Laws

Light can be described both, as an electromagnetic wave [wave theory (Webb 2005)], as well as particles [corpuscular (Demtröder 2010)]. Heinrich Hertz was the first who experimentally discovered the photoelectric effect but Einstein was the one who explained this effect later. The dualism of light is reflected in the combination of two fundamental laws of physics, and the energy of a photon W can be described by its frequency or its mass m_p:

$$W = hf \quad \text{(Plancks law)} \tag{2.1}$$

$$W = m_p c_0^2 \quad \text{(Einstein)} \tag{2.2}$$

c_0 speed of light in vacuum and
h Plancks constant.

By combining both equations, one can determine the DeBroglie-wavelength (Demtröder 2010) which allocates every particle of mass m and the velocity v with an adequate wavelength:

$$\lambda_0 = h/(mv) \quad \text{(DeBroglie)} \tag{2.3}$$

U.H.P. Fischer-Hirchert, *Photonic Packaging Sourcebook*,
DOI 10.1007/978-3-642-25376-8_2

2.1.1 Homogeneous Plane Wave

A wave can be described by a sinus function. First, we shall confine to the stationary time-dependent treatment:

$$g(t) = a\cos(2\pi f t + \phi) \tag{2.4}$$

a amplitude
$(2\pi f t + \phi)$ phase

or in complex numbers:

$$g(t) = a\cos(t + \phi) = a\,\mathrm{Re}\left\{e^{j(t+\phi)}\right\} = \mathrm{Re}\left\{Ae^{jt}\right\} \tag{2.5}$$

with complex amplitude; $A = ae^{j\phi}$

More important optical basics:

$$\omega = 2\pi f \quad \text{frequency} \tag{2.6}$$

$$t_p = 1/f \quad \text{time of oscillation} \tag{2.7}$$

$\lambda_1 = c_1 t_p = c_1/f$ light speed in wave length 1
$c_1 = c_0/n_1$ light speed in material 1
$n_1 = c_0/c_1$ Refractive index in material 1
$k_1 = k_0 n_1 = 2\pi n_1/\lambda_0$ wave number in material 1

Example: Frequency of the optical wave at 1.55 μm

$$f = c_0/\lambda = \left(3\times10^8\,\mathrm{m/s}\right)/\left(1.55\times10^{-6}\mathrm{m}\right) = 1.935\times10^{14}/\mathrm{s} = 193.5\times10^{12}\,\mathrm{Hz}$$

An overview of the exact name of m, s, and oscillation frequency is listed in the following Table 2.1.

Furthermore, the propagation direction e of the wave has to be determined when an additional spatial dependence of the wave is used as well. The coordinate system with the radius vectors $r(x, y, z)$ is chosen in such a way, that e is coincident with the z-direction as shown in Fig. 2.1.

$$\mathbf{r}e = \text{const} = \mathbf{r}\cos(\mathbf{r}, e) \tag{2.8}$$

This generates a plane that is perpendicular to the z-direction. The phase of the wave vector of a plane wave is constant within a site-fixed or time-fixed plane!

Table 2.1 Time and frequency units

Frequency units 1 Hz = [1/s]		
kHz	Kilohertz	10^3 Hz
MHz	Megahertz	10^6 Hz
GHz	Gigahertz	10^9 Hz
THz	Terahertz	10^{12} Hz
PHz	Petahertz	10^{15} Hz
Time units in seconds [s]		
ms	Millisecond	10^{-3} s
μs	Microsecond	10^{-6} s
ns	Nanosecond	10^{-9} s
ps	Picosecond	10^{-12} s
fs	Femtosecond	10^{-15} s
as	Attosecond	10^{-18} s

$$c_1 t \pm (re) = \text{const}$$

Complex:

$$\mathbf{E}(t) = \mathbf{A}e^{jt}$$

or with the spatial dependence:

$$\mathbf{E}(t) = \mathbf{A}\exp\{j(wt - rk)\} \tag{2.9}$$

This is the general description of the electric field vector **E**. The magnetic field **H** can be deduced analogously.

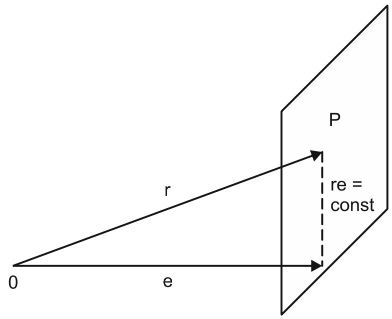

Fig. 2.1 Propagation of an electromagnetic wave

2.1.2 Phase and Group Velocity

The phase velocity (Demtröder 2010) of light can exceed the group velocity, especially in dispersive media. The behavior of group and phase velocities in quartz (Brooker 2003) is shown in Fig. 2.2. The group velocity is corresponding to the derivation of the refractive index of the medium in which the light propagates. The group refractive index describes the propagation of pulses in the medium, which may contain many frequency components according to Fourier (Bloomfield 2000). The group refractive index is usually higher than the phase refractive index, as shown in Fig. 2.2.

$$c_{\mathrm{ph}} = w/k_1 = c \quad \text{phase velocity} \tag{2.10}$$

$$v_{\mathrm{gr}} = \mathrm{d}w/\mathrm{d}k_1 = -\lambda^2 \mathrm{d}\omega/\mathrm{d}\lambda + c \quad \text{group velocity} \tag{2.11}$$

2.1.3 Reflection

The reflection is a process in which a beam of light which hits a reflective surface is reflected at the same angle, as at the incidence (see Fig. 2.3):

Angle of incidence = angle of reflection; $\alpha_1 = \alpha_2$

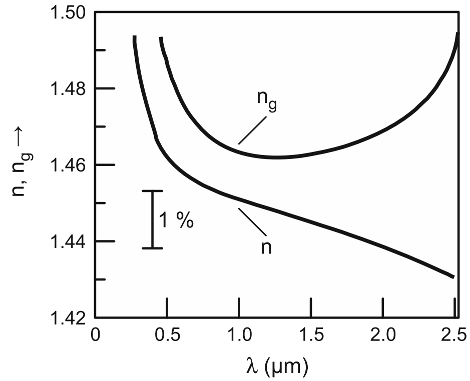

Fig. 2.2 Phase and group velocity of light in quartz

Fig. 2.3 Reflection of light

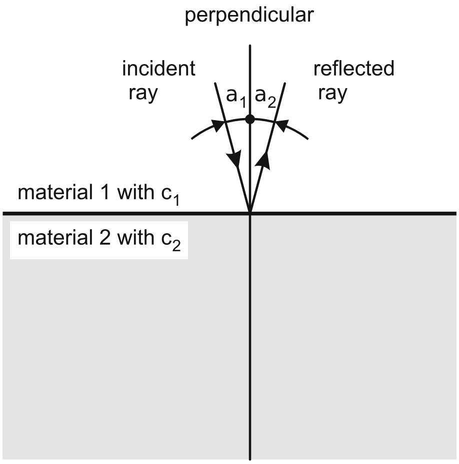

2.1.4 Refraction

Refraction (Fig. 2.4) eventuates when the light beam from a medium with a lower refractive index reaches a medium with higher refractive index.

There, it is broken off from the incidence perpendicular, due to the fact that the exit angle is larger than the incidence angle. The refractive indices are in medium $1n_1$ and in medium $2n_2$.

c_1 velocity of light medium 1
c_2 velocity of light medium 2

Fig. 2.4 Optical refraction

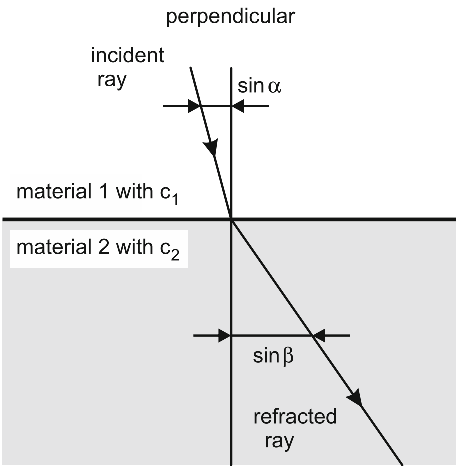

Example $n = 1.5$ of glass fibers

$$c_1 = c_0/n = \left(3 \times 10^8\ \text{m/s}\right)/1.5 = 2 \times 3 \times 10^8\ \text{m/s} = 200/\mu\text{s or } 5\ \text{ns/m}$$

This leads to Snell's (Brooker 2003) law of refraction:

$$\frac{\sin\alpha}{\sin\beta} = \frac{c_1}{c_2} = \frac{n_2}{n_1} \tag{2.12}$$

2.1.5 Total Reflection

From a critical angle α_0, the refracted beam 2 (Fig. 2.5) proceeds parallel to the interface between medium 1 and medium 2. During the transition from an optical denser medium to an optical thinner medium, the following condition applies to the total reflection angle (Brooker 2003):

$$\sin\alpha_0 = n_2/n_1$$

Example Refractive index of water = 1.333 against air $n = 1$

$$\sin\alpha_0 = 1/1.333 = 0.75 \quad \text{and} \quad \alpha_0 = 49^\circ$$

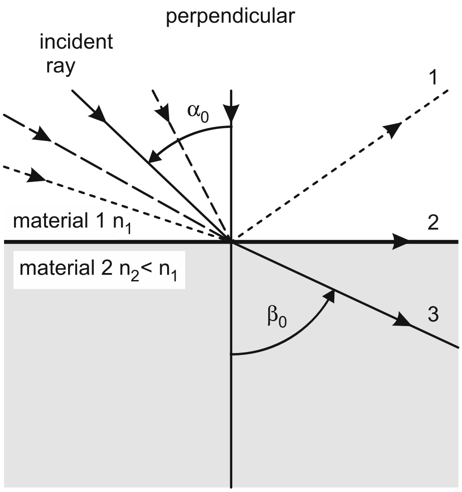

Fig. 2.5 Total optical reflection

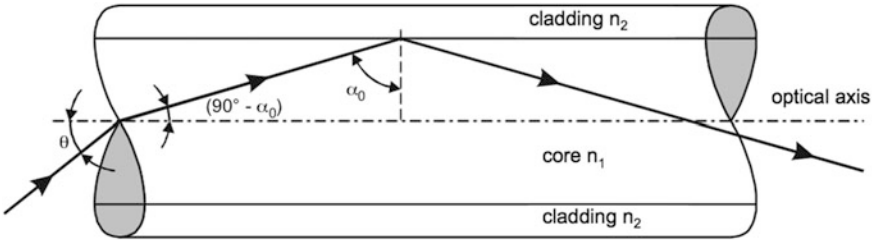

Fig. 2.6 Guided light in the fiber

2.1.6 Numerical Aperture

In the fiber, the light is guided through different refractive indices of the shell and the core, which suffice the following equation (see Fig. 2.6).

$$\sin \alpha_0 = n_2/n_1$$

To inject a light beam into the fiber, which can be guided in the core, the following equations are useful:

$$\sin \Theta / \sin(90^\circ - \alpha_0) = n_1/n_0;$$

with $n_0 = 1$ and sin(90∅−x) = cos(x) one has

$$\sin \Theta = n_1 \cos \alpha_0 = n_1 \mathrm{SQRT}\left(1 - \sin^2 \alpha_0\right)$$

from $\sin \alpha_0 = n_2/n_1$ follows the numerical aperture (NA) (Demtröder 2010) which can be seen in Fig. 2.6:

$$\sin \Theta = \mathrm{SQRT}\left(n_1^2 - n_2^2\right) = \mathrm{NA} \qquad (2.13)$$

2.2 Optical Fiber Profiles

When we consider the refractive index n of an optical fiber as a function of radius r, there is talk of the refractive index profile (Brooker 2003) of the optical fiber. Thereby, it is described the radial change of the refractive index of the optical fiber axis in the core glass to the outside in the direction of the coat glass (Fig. 2.7):

$$n = n(r)$$

$$n^2(r) = n_1^2[1 - 2\Delta(r)^g] \quad r < \text{a in core} \qquad (2.14)$$

Fig. 2.7 Refractive indexprofile of waveguides

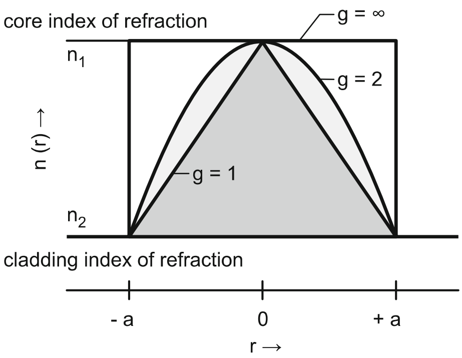

$$n^2(r) = n_2^2 = \text{const} \quad r > \text{a in cladding} \tag{2.15}$$

n_1 Refractive index at the fiber axis in microns (r = 0)
Δ normalized difference of the refractive index
r distance from fiber-optic cable axis in µm
a nuclear radius in µm
g potency, also called profile exponent
n_2 Refractive index of the cladding

The normalized difference in refractive index can be expressed as follows:

$$\Delta = \frac{(\mathrm{NA})^2}{2n_1^2} = \frac{n_1^2 - n_2^2}{2n_1^2} \tag{2.16}$$

Special cases:
$g = 1$ Triangle profile
$g = 2$ Parabola profile
$g \to \infty$ Step profile (marginal case)

Only in the latter case—the step profile—is the refractive index $n(r) = n_1$ = constant in the core glass. In all other profiles, the refractive index $n(r)$ increases in the core glass gradually (gradually increasing) of the value of n_2 of the cladding glass to the value n_1 of the fiber-optic axis (Fig. 1.7).

In case that you want to calculate the number of modes in a waveguide, you have to calculate at first the **V-parameter** (Marcuse 1974) or calculate the normalized frequency of the light in the waveguide:

$$V = \left(\frac{2\pi a}{\lambda}\right)\sqrt{\left(n_1^2 - n_2^2\right)} = k \cdot a \cdot \mathrm{NA} \tag{2.17}$$

a core radius,
λ wavelength,
NA numerical aperture,
k wavenumber, and
Δ normalized difference of the refractive index.

Example for the calculation of the V-parameter

$2a = 50\ \mu\text{m}$
$\lambda = 1550\ \text{nm}$

$$V = \left(\frac{2\pi 50\ \mu\text{m}}{1.55\ \mu\text{m}}\right)\sqrt{(1.48^2 - 1.46^2)} = \pi(50\ \mu\text{m}/1.55\ \mu\text{m})0.242 = 24.52 \quad (2.18)$$

The number of modes is generally calculated as follows:

$$\text{Step-index fibers:} \quad N = V^2/2 \quad (2.19)$$

$$\text{Graded-index fibers:} \quad N = V^2/4 \quad (2.20)$$

Example of calculating the number of modes:
$g = 2$
Graded-indexfibers $N = 82^2/2 * 2/4 = 1681$ modes
Step-index fibers $N = 82^2/2 = 3362$ modes

2.2.1 Step Profile

Figure 2.8 displays a typical multi-mode step waveguide. Typical dimensions for a multi-mode fiber with a stepped profile are the following internationally standardized (ITU 1994) dimensions:

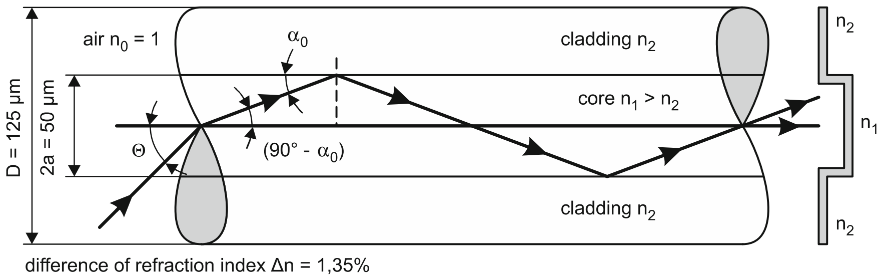

Fig. 2.8 Step-index waveguide

Core diameter	$2a$	50 mm
Cladding diameter	D	125 mm
Core number	n_1	1.48
Refractive index of the cladding	n_2	1.46
Difference of the refractive index	Δn	1.35 %

The critical angle α_0 characterizes the total reflection, i.e., the smallest angle to the perpendicular incidence at which a light beam is guided in the core glass and not broken in the cladding glass, which is shown in this example:

$$\sin \alpha_0 = \frac{n_2}{n_1} = \frac{1.46}{1.48} = 0.9865$$
$$\alpha_0 = 80.6^\circ$$
$$\sin \alpha_0 = \sqrt{n_1^2 - n_2^2} = \sqrt{1.48_1^2 - 1.46_1^2} = 0.242$$
$$\theta = 14^\circ$$

Since the sinus of the acceptance angle is defined as NA, the following is determined as:

$$\mathrm{NA} = \sin \theta = 0.242$$

Example:
An optical fiber with step profile of 1 km length is traversed in about 5 µs of light. The *time difference* (Ramaswami and Sivarajan 2004) Δt between the mode with the fastest and slowest distance in the conductor can be approximately estimated by the difference of the refractive index between core and cladding as shown below:

$$\Delta t = 5\,\mathrm{ms} \times \Delta n = 5 \times 10^{-6}\,\mathrm{s} \times 0.01 = 50\ \mathrm{ns}$$

If we assume a data rate of 1 MHz, the pulse will have a maximum allowable width of one µs. The distortion of the duration of the individual modes is called mode dispersion. In this case, this would be 1/20 of the data rate. This causes that the different spatial modes arrive at the end of the transmission line at different times and therefore, the original short incoming pulse will be extended at the outcome. Furthermore, this leads to a pulse widening at the receiver and this results in that the consecutively coming pulses cannot be separated properly which leads to an increasing rate of error.

2.2.2 Monomode Glass Fibers

The one-mode fiber-optic cable is also known internationally as single-mode fiber (SMF) (Ramaswami and Sivarajan 2004). Typical dimensions for a SMF are shown in Table 2.2.

The next Fig. 2.9 illustrates the path of a beam. To describe the light propagation of these small waveguide dimensions exactly, it is essential to use the wave theory of light.

In such a perspective the light propagates in the waveguide with a radial intensity distribution, which can be described by a very good approximation with a Gaussian function. This picture displays an intensity profile for a bimodal wave propagation (Ramaswami and Sivarajan 2004) which is shown in Fig. 2.10. It should be noted that the intensity distribution reaches up to the cladding.

Table 2.2 Single-mode fiber parameters

Mode field diameter	$2d$	8.5 µm
Outer diameter	D	125 µm
Core index	n_1	1.46
Index difference	Dn	0.003 = 3 ‰

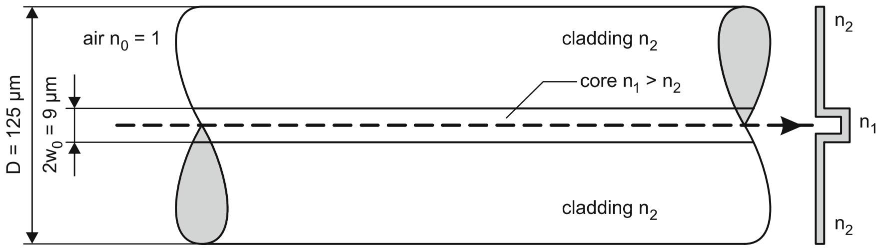

Fig. 2.9 Single-mode fiber

Fig. 2.10 Radial distribution of the fundamental mode LP01 at 1300 and 1550 nm

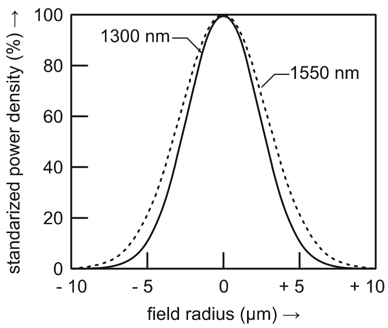

For a more detailed description of the Gaussian wave propagation in waveguides, see Chap. 3. A typical single-mode fiber-optic cable has the following NA:

$$\mathrm{NA} = n_1\sqrt{2 \times 0.003} = 0.113$$

Therefore, the acceptance angle Θ is calculated as follows:

$$\sin\theta = \mathrm{NA} = 0.113$$
$$\theta = 6.5^\circ$$

It should be noted that not only the core diameter, but also the NA, and therefore the angle of acceptance compared to the multi-mode-stepped profile fiber is considerably smaller whereby the coupling of light in the single-mode fiber-optic cable (see Chap. 4) is relatively difficult. The marginal wavelength, at which the SMF becomes multimodal, is generated in the following way (Mahlke and Gössing 1994; Ramaswami and Sivarajan 2004):

$$\lambda_c = \pi\frac{2a}{V_c}\mathrm{NA} = \pi\frac{8.5\ \mu\mathrm{m}}{2.405}0.113 = 1.255\ \mu\mathrm{m} \tag{2.21}$$

Example:
A single-mode optical fiber with step profile and a core diameter $2a$ = 8.5 μm and a marginal-wavelength λ_c = 1255 nm (Vc = 2.405) has a field diameter $2 \cdot w_0$ at the wavelength λ = 1300 and 1550 nm (see Table 2.3):

$$2 \cdot \omega_0 = \frac{2.6 \cdot \lambda}{V_c \cdot \lambda_c}2a \tag{2.22}$$

$$\lambda = 1300\,\mathrm{nm}: \quad 2\omega_0 = \frac{2.6 \cdot 1300\,\mathrm{nm}}{V_c \cdot 1255\,\mathrm{nm}}8.5\ \mu\mathrm{m} = 9.5\ \mu\mathrm{m}$$
$$\lambda = 1300\,\mathrm{nm}: \quad 2\omega_0 = \frac{2.6 \cdot 1550\,\mathrm{nm}}{V_c \cdot 1255\,\mathrm{nm}}8.5\ \mu\mathrm{m} = 11.3\ \mu\mathrm{m}$$

Table 2.3 Mode field diameter at different wavelengths ($2a$ = 8.5 μm)

Wavelength in nm	Mode field diameter in μm
1550	11.3
1300	9.5
1060	6.5
850	5.2
630	3.9

2.2.3 Gradient profile

Fibers with gradient profile have no step in the process of the refractive index but further parabola-shaped profile (Fig. 2.11). The advantage of this fact is that all the light beams in the waveguide need the same time over the transmission length because the product of the refractive index and optical path length can be kept constant. It does not matter whether the light beam is injected more flat or at a higher aperture. That means a significant increase of bandwidth for the signal in comparison to the step-index multi-mode fiber. The pulse that has to be transmitted does not run temporal wide apart because of the coordination of the propagation speed of the individual local modes as in the step-index fiber. However, the technical meaning of the gradient fibers is moved in the background because of the invention of the single-mode fiber with an improved transmission quality. Typical dimensions for a fiber-optic cable with a gradient profile (see Table 2.4) are :

For a typical fiber-optic cable with gradient profile, the NA is given as follows (Fig. 2.12):

$$NA = \sin\theta = \sqrt{n_1^2 - n_2^2} = \sqrt{1.46^2 - 1.606^2} = 0.206$$
$$\theta = 11.9°$$

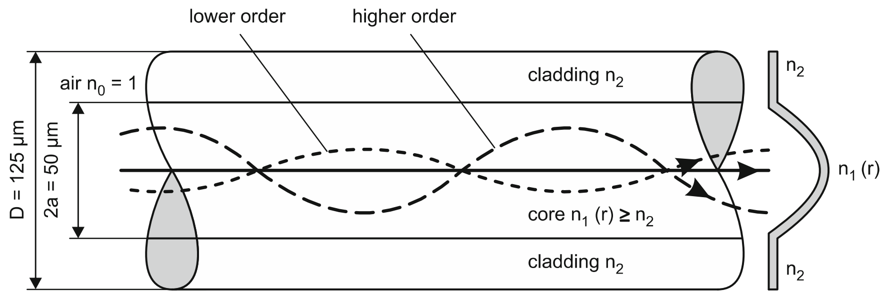

Fig. 2.11 Waveguide with parabolic refractive index profile

Table 2.4 Parameters of multi-mode glass fibers with gradient index profile

Core diameter	$2a$	50/62.5 µm
Cladding diameter	D	125 µm
Max. refractive index of core	n_1	1.46
Difference of refractive index between core and cladding	Δ	0.010

Fig. 2.12 Front facet of a single-mode glass fiber

2.2.4 Phase-space Diagrams: ($\sin^2\Theta$ *and* r^2)

A phase-space diagram describes the graphical representation of the square of the NA as a function of radial expansion of the waveguide (Fig. 2.13). It is a convenient tool for determining the coupling efficiencies (Marcuse 1977, 1978) between gradient fibers. The area below the marginal curve for the maximum angle of acceptance Θ_{max} is proportional to the fed-in light power in the core.

It is obvious that with the same NA and the same core radius a, this power is twice as large in a fiber-optic cable with step profile (Fig. 2.14) as in a fiber with a gradient profile (Fig. 2.15). These losses can be calculated as follows:

$$L_{MM} = -10\log\left[\frac{a_1}{a_2}\right]^2 \quad \text{with } a_1 > a_2 \tag{2.23}$$

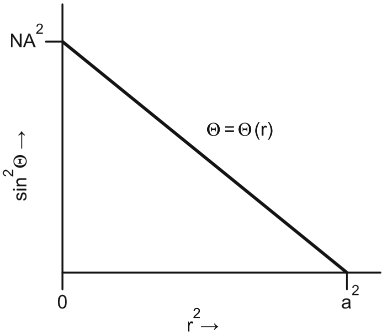

Fig. 2.13 Phase diagram of a gradient indexglass fiber

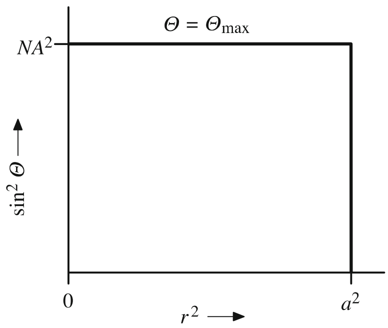

Fig. 2.14 Phase diagram of a waveguide with step-index profile

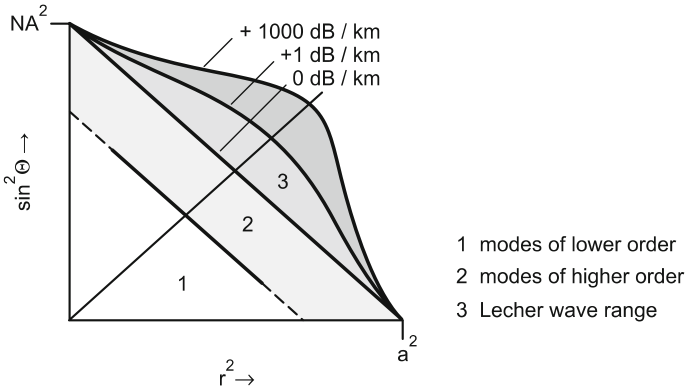

Fig. 2.15 Different mode propagation losses shown by a phase diagram

The behavior of the propagable modes in the multi-mode fiber-optic cable is plotted in Fig. 2.15. Modes with a lower order spread more in the core center, while the higher order modes spread out more near by the cladding. Leaky wave modes (Geckeler 1990) are also indicated, but have an extremely high attenuation of 1000 dB/km.

2.3 Dispersion

One has to consider two types of dispersion in glass fibers:

(a) Material dispersion
(b) Waveguide dispersion

Both types of dispersion together are called chromatic dispersion. In the wavelength range larger than 1300 nm, both fused silica dispersions have an

Fig. 2.16 Chromatic dispersion as a function of wavelength in glass fiber

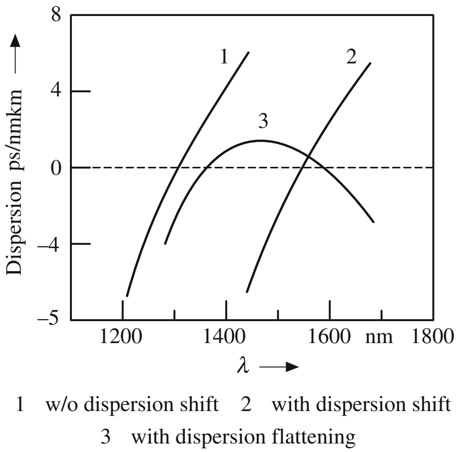

opposite sign. The material dispersion can be changed only slightly by other glass endowments. On the other hand, it is possible to influence the wavelength dispersion essential through a different structure of the refractive index profile.

Figure 2.16 displays dispersion behavior for three differently endowed glass fibers. Moreover, curve 1 shows the process of the dispersion of a standard fiber according to Mahlke and Gössing (1994). The behavior of a suspended dispersion fiber is shown in curve 2. Therefore, in the frequency range of 1550 nm, there is a very low dispersion to increase the transmission rate at this point. Curve 3 illustrates the process of another variant of optical fibers, the dispersion smoothed fiber. Thereby, one can reach a preferably low dispersion in a wide spectral range that can be advantageous in a wavelength multiplex system because many transmission channels see the same low dispersion.

2.4 Attenuation

The attenuation of the fiber is made up of several absorption parts, which can be seen in Fig. 2.17. A large proportion of the absorption of short wavelengths is based on the Raleigh-dispersion (Brooker 2003). The reason for this is the scattering of light by dipole molecules of the glass material. Moreover, the dispersion increases with the increasing frequency of light ($\sim\omega^4$). In addition, the glass absorbs strongly in the UV region because the offshoots of the absorption edges still need to be considered, but are negligible in the range of 1.55 μm. Roughness of the surface zone of the waveguide between core and cladding increase the attenuation slightly by a few thousandths of a dB per km. At higher wavelengths, the infrared absorption of the glass material limits the transmission range at 1.6 μm wavelength. Additionally, absorption peaks at 1.4 μm wavelength are recognized which are caused by OH-absorption of the glass.

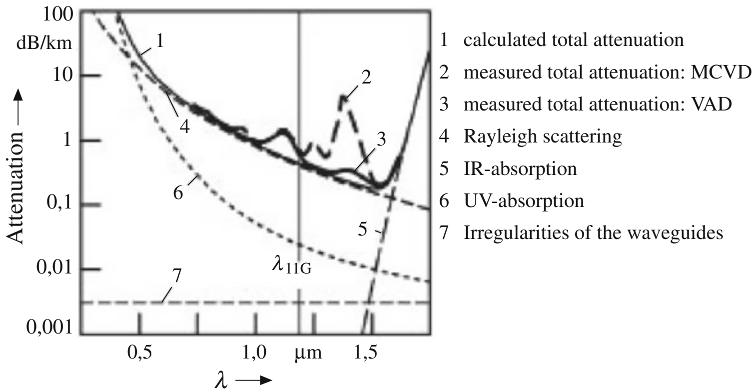

Fig. 2.17 Attenuation curves of glass fiber

In more recent fibers, it has been successfully implemented that these OH-radicals of the core region of the waveguide are squeezed out by a special tempering regulation that cause the disappearance of the absorption. These fibers are called "water free".

If one wants to extend the transmission range to longer wavelengths, it will be necessary to use other glass systems. Halogen glasses such as BaF_2-CaF_2-YF_3-AlF_3 and BaF_2-ZrF_4 GdF_3 or chalcogen glass (GeS_3) shows infrared absorption at wavelengths starting from 3 µm. Figure 2.18 shows the attenuation characteristic of these glasses (Grau and Freude 1991). The refractive index is presented with n_D regarding to the associated kind of glass which is measured at a wavelength of 589 nm. It is obvious that in contrast to SiO_2, it is possible to reduce the expected attenuation by two dimensions. However, at the moment, the high manufacturing costs of these glasses prevent the further spread outside the framework of the experiments in laboratories. Moreover, the long-term stability leaves a lot to be desired. Over time, these compounds gather water, which diffused into the fibers and in this way they pollute and change the characterizations massive.

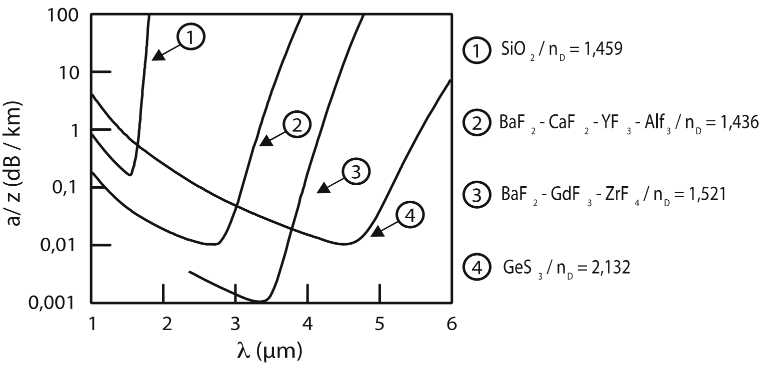

Fig. 2.18 Attenuation curves of halogen and chalcogen glasses

2.5 Polymeric Fibers

Indoors, in the automotive industry and in the range up to 100 m cable length, the following fibers are used: PMMA, polystyrene (PS) and polycarbonate (PC). The advantages in comparison with glass fibers are the low cost, the high flexural strength, and the easier treatment of the material. Apart from these values, the standard VDE 0888 part 101 describes more values such as mechanical, optical transmission, and technology values.

Minimum attenuation values (Fig. 2.19) of 80/km are achieved at a wavelength of 570 nm. At higher wavelengths, the attenuation values increase to more than 1000 dB/km, so that these fibers can be used only at short wavelengths and short distances due to the extremely high attenuation values.

Nowadays, recent variants with endowed PMMA reach attenuation values below 30 dB/km (D-PMMA). The material Cytop and mixtures of PMMA and SiO_2 already show attenuations below 5 dB/km, but the manufacturing is very expensive. The structure of the fiber is also very different compared with the glass fiber types; the core is very large but the cladding is very thin with a high refractive index jump of 0.5 %. The following characteristics describe this fiber type (Table 2.5).

In polymeric fiber systems, the NA is fixed to 0.5. This represents an aperture angle of 30°. Comparing POF to glass fibers, one can see the difference of the core

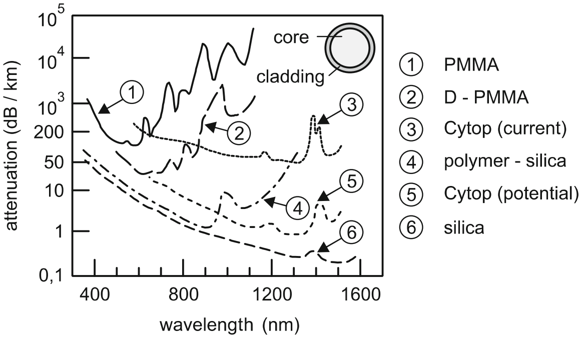

Fig. 2.19 Attenuation of different polymeric fibers

Table 2.5 Parameters of polymeric fibers for short-range optical transmission systems

Core diameter	480, 720, 980 μm
Refractive index	n_{core} = 1.492, n_{clad} = 1.412
Cladding diameter	500, 750, 1000 μm
NA	0.5
Transport and storage temperature	−40 bis 85 °C
Installation temperature	5 bis 40 °C
Operating	−40 bis 85 °C
Minimum attenuation	80 dB/km (PMMA/570 nm)

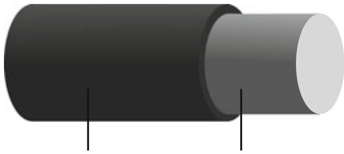

Fig. 2.20 Polymeric step-index fiber

and cladding refractive indices is 5 %. The NA is correlated by the normalized parameter V. The V-parameter is a correlation to the number of optical modes in the optical waveguide. The number of the modes, which are confined in a fiber, can be determined by the relationship between the wavelength of the light passing through the fiber, the core diameter, and the material of the optical waveguide. This relationship is known as the normalized frequency parameter, or V number shown in Eq. (2.17).

Standard single-mode fibers typically have a V number that is about 2.405. Here, the light will propagate in only one single mode. On the other hand, in multi-mode step-index POF fibers (Fig. 2.20), the V number is 2.799, at of yellow/550 nm, core radius of 490 µm, and NA of 0.5. This is more than 10^3 times larger than for single-mode fibers. In this case, the light will propagate in many paths or modes via the fiber. The count of optical modes for step-index POFs will be extracted to $N = V^2/2 = 3.917$ Mio modes. Using higher wavelengths, the number of modes will reduce to 2.804 Mio modes at red/650 nm. By this reasons, POFs are only introduced in short-range transmission systems using distances between 1 m and 100 m.

2.6 Optical Waveguides in InP, GaAs, PMMA, and SiO_2

In addition to the radial symmetric waveguides, which are discussed in the previous sections, optical waveguides are mainly used in semiconductor technology. The reason behind this is that the coatings and endowments are always applied in layers in the semiconductor material, and the radial symmetric structures can only be realized with great effort.

The propagation in a waveguide layer (Fig. 2.21) is realized by reflection on the two marginal surfaces, similar to a radial waveguide. The side of the boundary of the waveguide gives the extension in the width. Different forms of layer waveguides are given as follows:

- rib waveguides
- buried waveguides
- inverse rib waveguide.

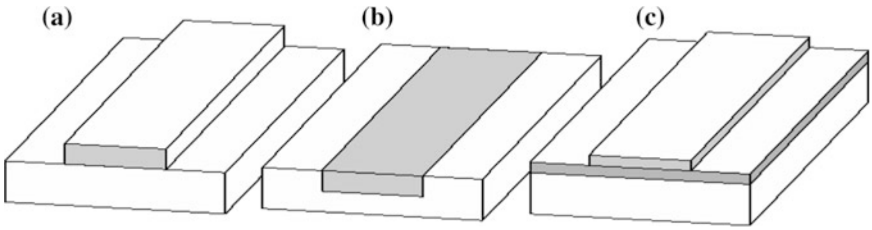

Fig. 2.21 **a** Rib waveguide, **b** buried waveguide and **c** inverse rib waveguide

Active elements are produced in the quaternary material system consisting of III–V semiconductors: indium, gallium to aluminum, arsenic, and phosphorus. Passive elements are made of glass, SiO_2, and lithium niobate ($LiNbO_3$). The latter is widely used in the manufacturing of optical modulators in the gigahertz range.

A visual representation of the modus guide in a layer waveguide is shown in Fig. 2.22. One can see that the guide can be explained analogous to the glass fibers. The calculation of the modus propagation in the layer waveguides is nowadays done with the aid of complex programs, the so-called beam-propagation programs (He and Shi 2010; Paltani and Medhekar 2010) (BPM, see Chap. 12). These programs calculate the propagation of the electromagnetic wave with very small steps in the waveguide and display the intensity distribution of the wave over the entire waveguide.

A typical example for the calculation of a Mäandercoupler is illustrated in Fig. 2.23. The field distribution of a rip waveguide is calculated in several local modes. Here, too, the share of the wave is guided in the cladding, which is used in the optical coupler. Thereby, two waveguides are brought together so close, in which the light wave can be coupled from one waveguide to another. The Mäandercoupler uses several serpentine approximations of two waveguides to achieve the goal that the light of the right waveguide is completely transmitted to the left waveguide.

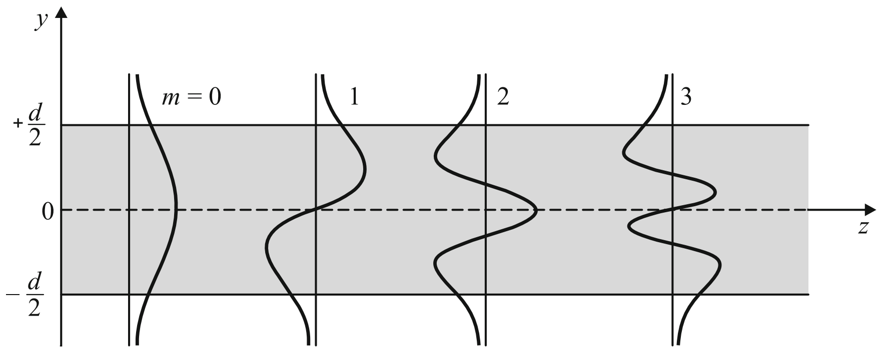

Fig. 2.22 Guided modes in a rib waveguide

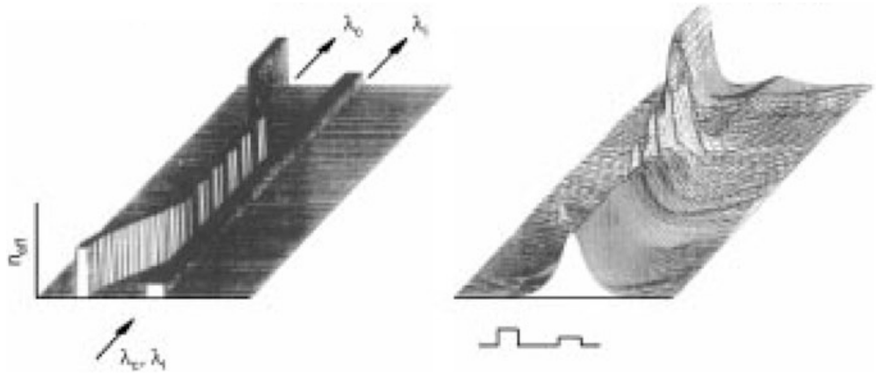

Fig. 2.23 Simulation of an optical waveguide in a 3 dB splitter, *left* effective index profile, *right* BPM simulation

2.6.1 Geometry of Integrated Waveguides

The waveguide of a layer structure in the InP system has the typical dimensions of 0.2 μm × 2 μm and generates at the waveguide end a highly asymmetrical elliptical field (Fig. 2.24). Therefore, it is necessary to realize a field adjustment to the fiber through a lens or a lens system. An example of the calculated field of a rib waveguide in InP is shown in Fig. 2.25.

In contrast to the rib waveguide, the buried waveguide (Fig. 2.25) field distribution in a rib waveguide with thickness of 0.11 μm, width 3 μm.

Figure 2.26 guides the wave through the middle of the waveguide, which makes the distribution of intensity of the field symmetrical. The field distribution of the rib waveguide is asymmetric concerning the y height. The main intensity of the light is not guided in the rib, but in the material underneath the rib, the bulk material. Curvatures of the waveguide without large radiation losses are impossible for the rip waveguides in contrast to the buried waveguides. Therefore, one prefers buried waveguides for monolithic integrated circuits because smaller curvatures allow a higher packing density in the circuit and thereby the required area and costs for a component decrease.

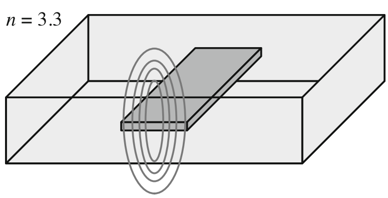

Fig. 2.24 Optical field distribution of a buried waveguide

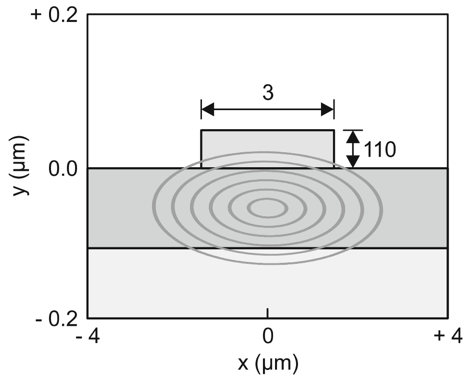

Fig. 2.25 Field distribution in a rib waveguide with thickness of 0.11 µm, width 3 µm

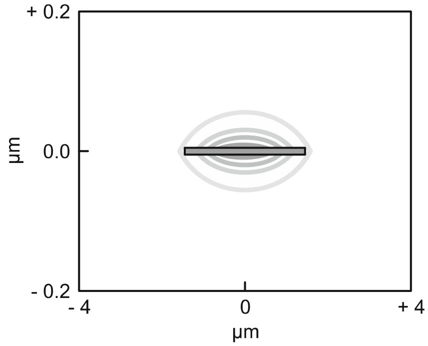

Fig. 2.26 Field distribution in a buried waveguide with width of 3 µm and thickness of 110 nm

2.6.2 Semiconductor Laser

The layer structure of a semiconductor laser is illustrated schematically in Fig. 2.27. The figure shows a buried waveguide in which lies simultaneously the active zone. In this zone, the charge carriers are generated, which emit light when they are recombined (Fischer 2002). The slit edges of the chip form the laser mirrors at the same time which reflect approximately 30 % air in InP components. In the present example, the boundary of the active region is caused by the size of the electrical connection field. At the same time, the active zone has a thickness of 0.2. The optical field of such a laser on the surface of the gap plane is shown in Fig. 2.28.

With an expansion of 4.7 µm in vertical direction and 2.5 µm in lateral direction, the field is distributed very asymmetric. The larger dimension in the vertical direction is due to the fact that the field still breaks very low in the bulk material and is transmitted in the following, whereas the lateral boundary is retained well because of the mechanical-defined parameters.

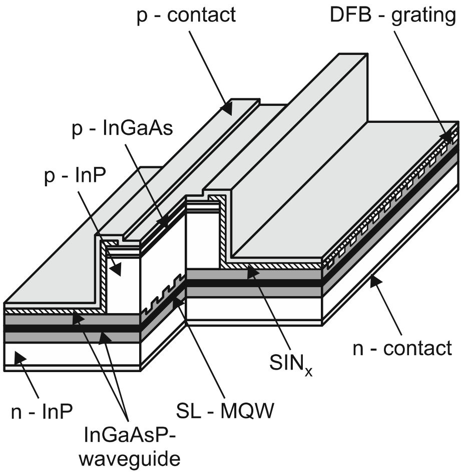

Fig. 2.27 Semiconductor multi-quantum well (MQW) laser with distributed feedback grating (DFB)

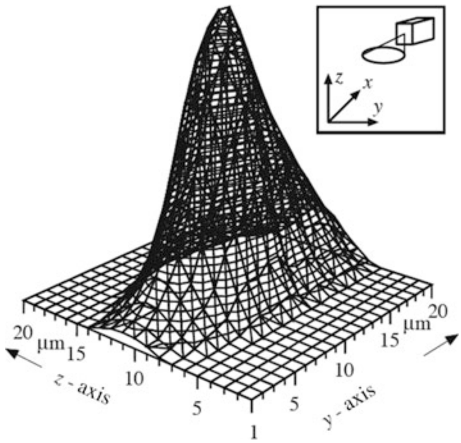

Fig. 2.28 Near-field distribution of a DFB laser diode with mode field widths of 4.7 µm horizontal and 2.5 µm vertical

2.6.3 PMMA-integrated Waveguides

This type of waveguide is used for passive structures. Figure 2.29 shows the layer structure. Out of it, one can manufacture optical splitters, switches, etc. The production of this kind of layer waveguides is achieved by hurling in the centrifuge.

The liquid material is applied to the base material, in this case silicon, and then hurled with about 1000 revolutions per minute. Now, it is formed a thin polymer film whose thickness is a direct function of the rotational speed and time. Therefore, the thickness of 1–30 µm can be applied well-controlled layer by layer. Many different optical devices like AWGs, thermal switches or multi coupler structures have been shown by several groups in Germany (Keil et al. 1996, 2001; Yao et al. 2002) and Korea (Kim et al. 2007a, b; Lee 2012).

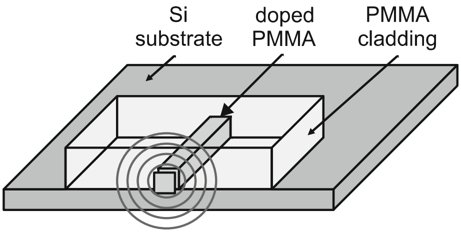

Fig. 2.29 Sandwich layer setup and optical field distribution of an integrated PMMA waveguide

The lateral structure is achieved by photolithography. Therefore, a chrome mask is placed on the substrate, in which the waveguide structure is kept free. In the following, the photophobic material is exposed with UV light, which leads to an increasing of the refractive index at the exposed places. A subsequent thermal treatment results in an evaporation of the remaining photosensitive endowment material. In a further step, it is possible to hurl up a cladding layer with a lower refractive index than the waveguide material of the waveguide layer. All working steps are shown in Fig. 2.30.

The characterizations of the resulting waveguides in PMMA are listed below:

- Waveguide 8 μm × 8 μm,
- Symmetrical field,
- Good field adaptation to optical fiber with a
- Refractive index difference of $n_{\text{Clad}} = 1.51$–$n_{\text{core}} = 1.53$.

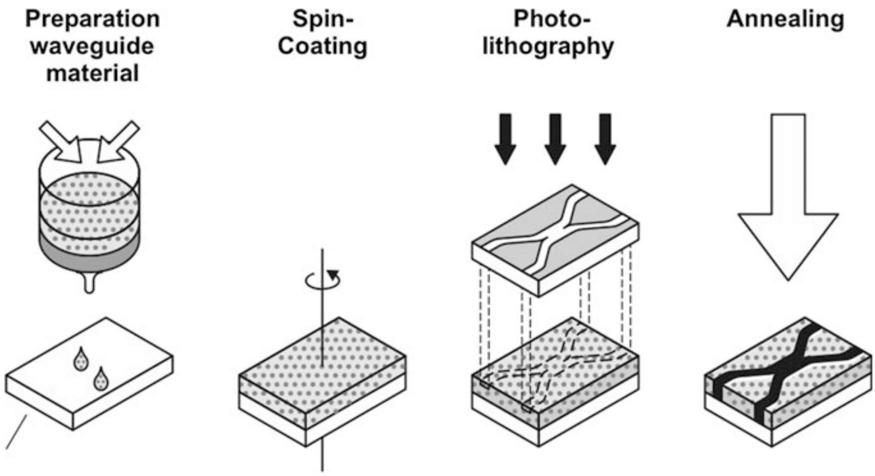

Fig. 2.30 Fabrication process of PMMA layers

2.7 SiO_2-Optical Waveguides

SiO_2 waveguides (Kilian et al. 2000) are also used at layer waveguides for passive structures. The waveguide dimensions are 6 μm × 6 μm in width and height, with a refractive index jump of 4 % at a core refractive index of n_{core} = 1.447. The symmetry of the waveguide leads to a very symmetrical field with a good field adaptation to glass fiber.

For the production of these waveguides, the base material is again the silicon substrate. Upon this, we evaporate a layer of silica (SiO_2) by flame (Kawachi et al. 1983; Kominato et al. 1990; Bebbington et al. 1993; Kilian et al. 2000; Garcia-Blanco et al. 2004). Therefore, a mixture of the required materials is heated in an oxyhydrogen container. In the following, Si and O_2 are bonded to SiO_2 by chemical reaction and with other endowment materials, which are required for refractive index settings, they settle themselves down. After that, a mask is applied to the wafer that is connected to the waveguide strip (negative mask). Through these openings, it is possible to skim the material through reactive ion-etching. After removing the mask, the rest of the waveguide plank stands alone. In a further step, another layer of glass (the cladding layer with about 30–50 μm thickness) is evaporated by flame hydrolysis on this surface. The result corresponds to the sequence of events which are in Figs. 2.31 and 2.32.

Thus, prepared SiO_2 waveguides have an expansion of 6 μm × 6 μm, a symmetric field and also a good adaptation to the field optical fiber with a refractive index of n_{Clad} = 1.447 with 0.7 % refractive index jump. Average losses in the fiber-chip coupling are less than one dB.

The attenuation at 1.55 μm is analogous to the optical fibers very low. However, the process is currently not satisfying to lead because water is still left in the material after the production process which influences the attenuation negative. Typical attenuation values with different endowment materials are given as follows:

$$\begin{aligned} SiO_2 - TiO_2 (Dn = 0.25\ \%) &: \quad 0.27\ \mathrm{dB/cm} \\ SiO_2 - GeO_2 (Dn = 0.75\ \%) &: \quad 0.04\ \mathrm{dB/cm} \end{aligned}$$

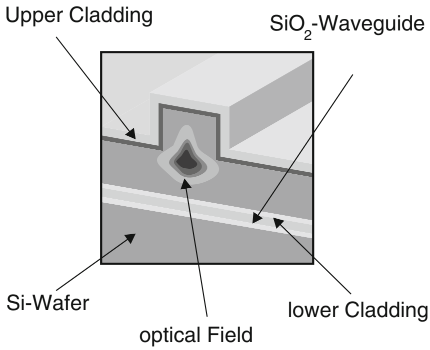

Fig. 2.31 Cross section of a silica waveguide with near-field distribution

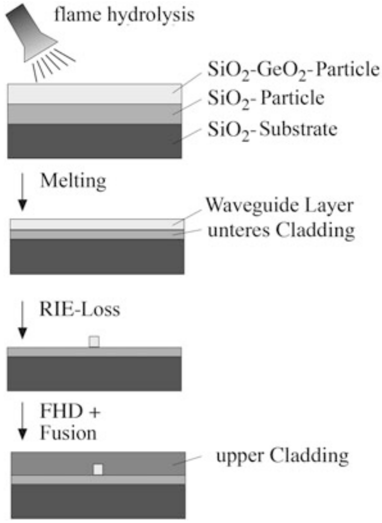

Fig. 2.32 Fabrication process of SiO_2 layers using flame hydrolysis

In summary, the properties of the silica waveguides in planar construction are listed below:

- Very low propagation losses (<0.05 dB/cm)
- Low temperature dependence of the refractive index ($dn/dT = 1.1 + 10^{-5}$) and therefore low thermal drift at ambient temperature.
- Thermally and mechanically stable
- Polarization-independent components can be realized
- Low-loss optical fiber coupling with non-critical alignment tolerances (±2 μm at 1 dB additional loss)
- It is possible to do an Er-doping of SiO_2 for the production of integrated optical amplifiers

2.8 Production of Optical Fibers

The production of a glass fiber consists—independent of the used method—always of two stages. The first step is the preparation of a preform which is shaped with easy mechanical methods (milling and spinning) and which is coated in an endowment machine with the refractive index of core and cladding. When we consider the profile of the preform, one can see a true to scale enlargement of the mechanical dimensions and of the refractive profile of the future glass waveguide.

In the following, the preform is stretched through a fiber stretch machine to a thickness of 125 μm and a plastic layer is immediately applied (primary coating). The necessary endowment of SiO_2 monomode fibers is done with additional

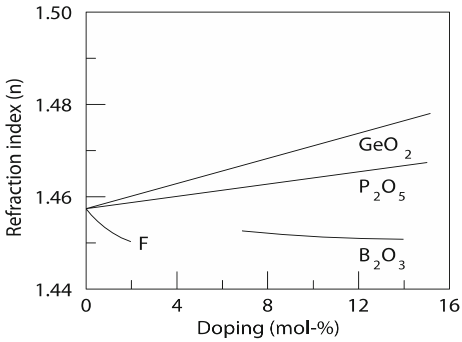

Fig. 2.33 Variations of refractive indices using germanium, phosphorus, or boron oxide

material to modify the refractive index of the core and cladding. Figure 2.33 illustrates the change of refractive index as a function of the endowment concentration of germanium, fluorine, and phosphorus oxide.

2.9 Gas Phase Methods

The manufacturing methods of extremely low-vapor glass fibers normally used today are achieved with the aid of separating processes from the gas phase that were developed in 1970 (Schultz 2010) by Corning scientists Dr. Robert Maurer, Dr. Peter Schultz, and Dr. Donald Keck, Corning Inc., USA. A distinction is made between three different methods of separation. If the separation is on the outside of a preform, the process is called the OVD method (Schultz 2010; Murata 1996) (outside vapor deposition). A process that carries out the separation on the facing side of a preform is called the VAD method (vapor axial deposition).

If the materials are deposited on the inside of a rotating glass rod, this is referred to as the IVD method (inside vapor deposition). In the latter IVD method, a distinction is made between the process where the required melt energy is supplied by oxyhydrogen burners, the MCVD method (modified chemical vapor deposition), and the method where the energy is supplied by a microwave source, the PCVD method (plasma-activated chemical vapor deposition).

In all methods, the deposition results from the decomposition of high-purity compounds in an oxyhydrogen flame. The gases required for this are listed in (Fig. 2.34) and belong to the group of chlorides, which, in turn, belong to the group of metal halides. Oxygen is fed into the burner together with the required doping agents and converted there into the corresponding oxides.

Oxygen is allowed to flow through vessel (bubblers), which contain liquid compounds at room temperature. Bubbles are formed and the oxygen, as the carrier gas, takes up the chlorides (Fig. 2.35). Due to the high level of heat energy supplied in the burner, the compounds are then converted into the corresponding oxides, which separate as a fine coating on the preform. If the burner is then also moved

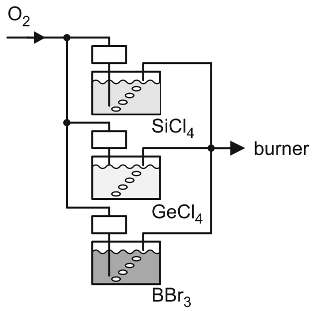

Fig. 2.34 Gas application for glass fiber preform fabrication

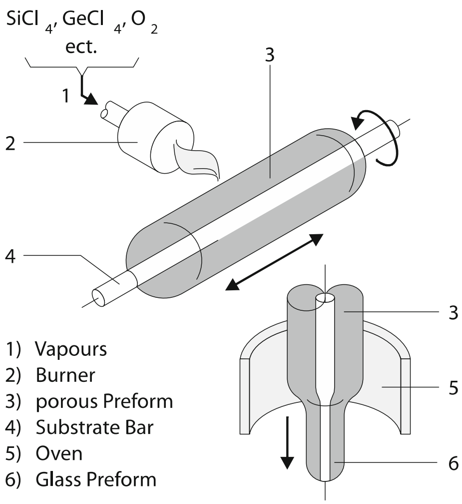

Fig. 2.35 Outside vapor deposition (OVD) technique

back and forth, a porous glass coating is formed in layers where each layer can be doped differently by varying the concentration of gases supplied. The outside vapor deposition method (OVD) is described below:

$$SiCl_4 + O_2 \rightarrow SiO_2 + 2Cl_2$$

And for germanium as the doping agent:

$$GeCl_4 + O_2 \rightarrow GeO_2 + 2Cl_2$$

The layers are deposited on the outside of the preform, hence the name "Outside." In the VAD method, a rotating glass rod is heated on the facing side with the burner and the gases separate there (Fig. 2.36).

The resulting form is slowly drawn upward where the distance from the burner to the form must always be kept constant. Several burners can also be used at the same time in order to coat the core and sheath simultaneously. Subsequent to the

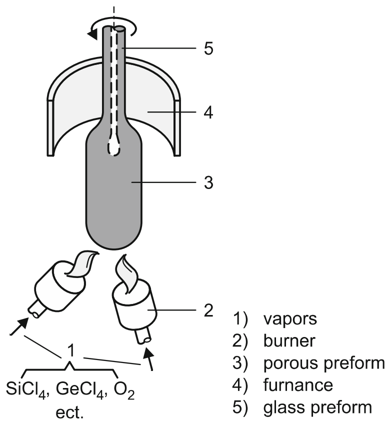

Fig. 2.36 Vapor outside deposition (VAD)

separation, the shrinking of the preform is then carried out via an annular heating arrangement. Chlorine gas is rinsed around the form for "drying," i.e., removal of water residues.

In MCVD (Fig. 2.37) and in the PCVD processes (Fig. 2.38), the gas flow is directed through a hollow preform so that the deposition occurs inside the form. The resulting temperatures are around 1600 °C which in the case of MCVD is generated by an oxyhydrogen burner and in PCVD by a microwave heater. Heating by microwave is particularly homogeneous and the layer sequence especially easy to control. In both methods, after applying the desired core layers, the glass is heated (2000 °C) until the form melts, thus shrinking it. No special drying processes are required, as no oxyhydrogen gas has been used inside the preform in either of the inner coating methods.

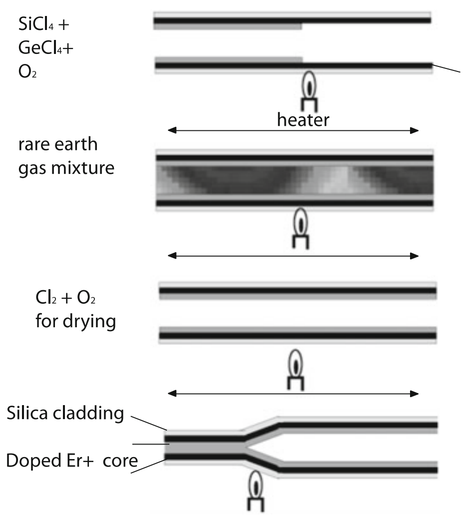

Fig. 2.37 MCVD technique (modified chemical vapor deposition)

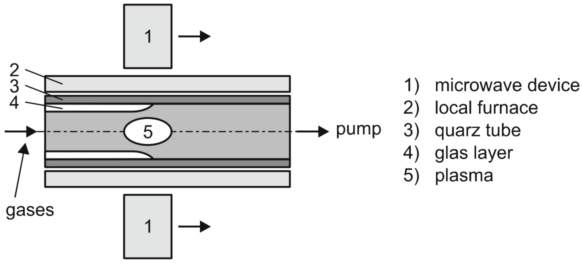

Fig. 2.38 PCVD process (plasma chemical vapor deposition)

2.9.1 Drawing of Glass Fibers

For extending the fiber, the finished base body (see Fig. 2.39) is hanged in a pull tower (Gehrke et al. 2009; Mahlke and Gössing 1994). The retainer is adjustable by *x*-, *y*-, *z*-positioning units. The height of such a tower is approximately 15 m. The end of the preform is heated to 200 °C and the next step is to grab the end and pull the fiber. The diameter of the fiber must be very consistent at 125 μm (±2 μm). To ensure this, the fiber diameter is measured online and therefore the pulling velocity and the heating temperature controlled accurately. During the drawing process, the geometric relationships of the preform remain stable so that a reduced image of the fiber preform is formed within the fiber with a corresponding refractive index profile.

Fig. 2.39 Fiber drawing tower

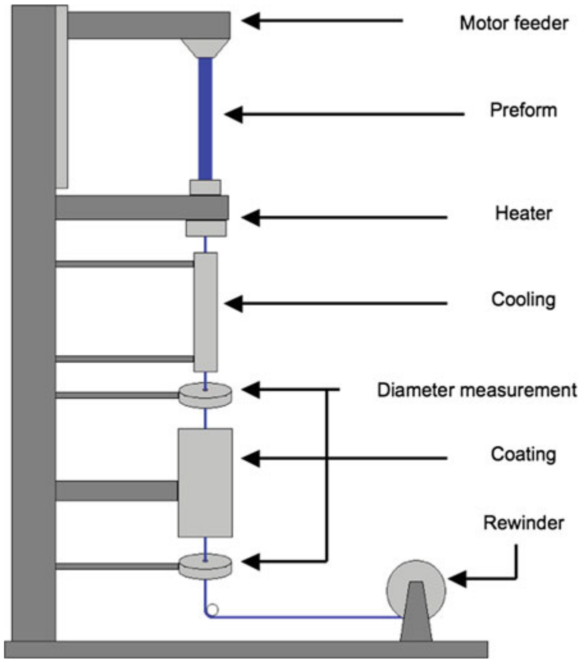

Aspect ratios of 400:1 are possible. Straight after the measurement of the fiber cross section, a first protective layer of PMMA is applied and immediately cured by ultraviolet light. This primary cladding layer is supposed to absorb the harmful environmental factors immediately after the manufacturing. Thus, the fiber diameter is summed up to a thickness of 250 μm. Then, the fiber is measured with a roller system, to test the tensile strength, and in the following, the fiber is wound up onto a cable drum.

2.9.2 Types of Fiber-Optic Cables

The finished fiber-optic cable needs further protection layers for the use in the field against bending, breaking, torsion, and tension. Therefore, the optic fiber is coated with a further protection layer, which can be varied depending on the requirement profile. The form and nature of the envelope is achieved through construction of cable technology. These are special structures of the fiber cladding and the installation of train and compression elements in the entire cable, such as steel wires or gel fillings.

Figure 2.40 illustrates several types of layer cables. There is a talk of a stranding at which rope elements are concentric organized around a central element. Cables with single elements such as glass fiber strands, copper strands, or others are called as plies cables. On the other hand, one speaks of bunched cable when the soul of a cable is setup of bunches of different elements. In the long-distance networks, there are mainly used plies cables and in the local network are used bunched cables.

Another variant of cables is ribbon cables. Therefore, a number of individual fiber-optic cables are fixed together to a flat band structure. Depending on the type of application, one distinguishes several different types, such as the ones in Fig. 2.40. These ribbon cables can be stacked in several layers and so you will reach a very high packing density.

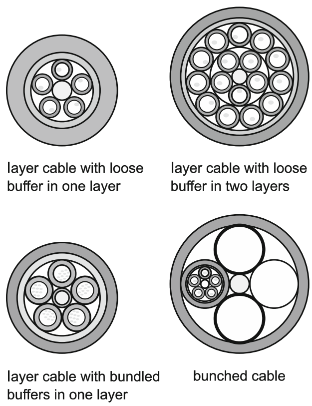

Fig. 2.40 Types of fiber-optic cables

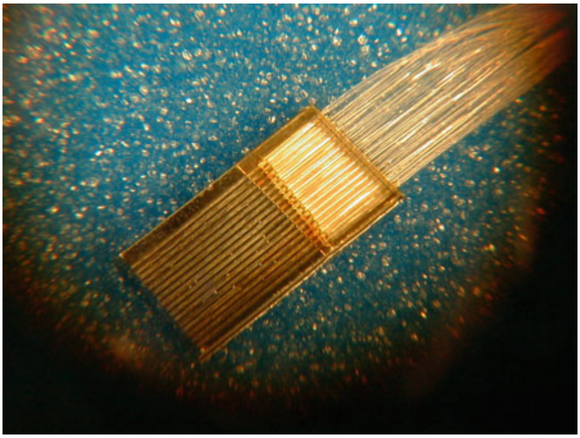

Fig. 2.41 Fiber-optic ribbon cable

The main application of this cable is located indoors at the direct connection to optical modules and components, such as Arrayed Waveguide Grating (AWG) modules. In such modules, the ribbon fiber is embedded and fixed to an array of silicon V-groove. This has the advantage to get a stable matrix of fibers with strong defined distance to the fiber-chip coupling (Fig. 2.41).

References

Bebbington, J.A., Barbarossa, G., Bonar, J.R., Aitchison, J.S.: Rare earth doped silica waveguides on Si fabricated by flame hydrolysis deposition and aerosol doping. Appl. Phys. Lett. **62**(4), 337–339 (1993)

Bloomfield, P.: Fourier Analysis of Time Series: An Introduction. Wiley Series in Probability and Statistics. Wiley, New York (2000)

Brooker, G.A.: Modern Classical Optics (Physics). Oxford University Press, Oxford (2003)

Demtröder, W.: Atoms, Molecules and Photons: An Introduction to Atomic-, Molecular- and Quantum Physics. Graduate Texts in Physics. Springer, Berlin (2010)

Fischer, U.H.P.: Optoelectronic Packaging. VDE, Berlin (2002)

Garcia-Blanco, S., Alfaro-Cid, E., De La Rue, R.M., Aitchison, J.S.: Genetic algorithm-based characterization of the optical properties of flame-hydrolysis deposited silica waveguides. J. Lightwave Technol. **22**(12), 2801–2807 (2004)

Geckeler, S.: Lichtwellenleiter für die optische Nachrichtenübertragung. Springer, Berlin, Heidelberg (1990)

Gehrke, N., Casper, A., Otto, O., Heinemann, R., Tockhorn, M., Fischer, UHP: Studie Zur Realisierung Eines Ziehturms Für Polymeroptische Fasern. In: 10 NachwuchsWissenschaftlerKonferenz, HS Merseburg (FH). HS Merseburg 2009

Grau, G., Freude, W.: Optische Nachrichtentechnik: Eine Einführung. Springer, Berlin (1991)

He, Y., Shi, F.: Beam Propagation Method and Microlens Design for optical Coupling. VDM Verlag Dr. Müller, Saarbrücken (2010)

ITU RG: Transmission Media Characteristics: Definition and Test Methods for the relevant Parameters of Single-Mode fibres. T94. ITU (1994)

Kawachi, M., Yasu, M., Edahiro, T.: Fabrication of SiO_2-TiO_2 glass planar optical waveguides by flame hydrolysis deposition. Electron. Lett. **19**(15), 583–584 (1983)

Keil, N., Yao, H.H., Zawadzki, C.: Polymer waveguide optical switch with < -40 dB polarisation independent crosstalk. Electron. Lett. **32**(7), 655, 657 (1996)

Keil, N., Yao, H.H., Zawadzki, C., Bauer, J., Bauer, M., Dreyer, C., Schneider, J.: Athermal all-polymer arrayed-waveguide grating multiplexer. Electron. Lett. **37**(9), 579–580 (2001)

Kilian, A., Kirchof, J., Przyrembel, G., Wischmann, W.: Birefringence free planar optical waveguide made by flame hydrolysis deposition (FHD) through tailoring of the overcladding. J. Lightwave Technol. **18**(2), 193–198 (2000)

Kim, J.T., Ju, J.J., Suntak, P. Myung-Hyun, L.: O/E integration of polymer waveguide devices by using replication technology. IEEE J. Sel. Top. Quantum Electron. **13**(2), 177, 184 (2007a)

Kim, J.T., Ju, J.J., Suntak, P., Koo, S., Kim, M.-S., Myung-Hyun, L.: UV-embossed polymer optical bench for integration of polymer waveguide devices. Digest of the IEEE/LEOS Summer Topical Meetings. pp.111–112 (2007b)

Kominato, T., Ohmori, Y., Okazaki, H., Yasu, M.: Very low-loss GeO_2 doped silica waveguides fabricated by flame hydrolysis deposition method. Electron. Lett. **26**(5), 327–329 (1990)

Mahlke, A., Gössing, P.: Fiber Optic Cables. Fundamentals, Cable Engineering, Systems Planning. Publicis Corporate Publishing (1994)

Marcuse, D.: Theory of Dielectric Waveguides. Academic Press, New York (1974)

Marcuse, D.: Loss analysis of single-mode fiber splices. Bell Syst. Tech. J. **56**, 15 (1977)

Marcuse, D.: Gaussian approximation of the fundamental modes of graded-index fibers. J. Opt. Soc. AM **68**(1), 103–109 (1978)

Murata, H.: Handbook of Optical Fibers and Cables, 2nd edn. Optical Engineering. Marcel Dekker Inc., New York (1996)

Paltani, P.P., Medhekar, S.: Optical Beam Propagation in Non-Linear Media and All-Optical Devices: Investigation of Light Beam Propagation in Non-Linear (NL) Media For All-Optical Devices (AODs). VDM Verlag Dr. Müller, Saarbrücken (2010)

Ramaswami, R., Sivarajan, K.: Optical Networks. Academic Press, San Diego (2004)

Schultz, P.C.: Title: Making the first low loss optical fibers for communications. In: 36th European Conference and Exhibition on Optical Communication, ECOC. Torino (2010)

Webb, R.H.: Elementary Wave Optics. Dover Books on Physics (2005)

Yao, H.H., Zawadzki, C., Keil, N., Bauer, M., Dreyer, C., Schneider, I.: Polymer waveguide devices. Lasers and Electro-Optics, 2002. CLEO '02. Papers Presented at the Technical Digest. Summaries. **1**, 489–490 (2002)

http://www.springer.com/978-3-642-25375-1

Photonic Packaging Sourcebook
Fiber-Chip Coupling for Optical Components, Basic Calculations, Modules
Fischer-Hirchert, U.
2015, XIX, 325 p. 287 illus., 16 illus. in color., Hardcover
ISBN: 978-3-642-25375-1